Zinc finger translocation-associated protein promotes ferroptosis through the upregulation of ACSL4 expression in vascular endothelial cells

HUI-XIN GAO, JUN JIANG, CHUN-YAN YANG, JIN-FU XU, QING HE and YAN-WEI HU

Department of Clinical Laboratory, Guangzhou Women and Children Medical Center,
Guangzhou Medical University, Guangzhou, Guangdong 510600, P.R. China

Abstract. Numerous studies have reported the potential involvement of ferroptosis in the development of atherosclerosis (AS). Acyl-CoA synthetase long chain family member 4 (ACSL4) is an essential component in the promotion of ferroptosis. The present study aimed to investigate the role of ACSL4 and zinc finger translocation-associated protein (ZFTA) in the regulation of endothelial cell ferroptosis in AS. Human umbilical vein endothelial cells (HUVECs) with ACSL4 knockout were generated using CRISPR/Cas9 technology. To assess ferroptosis, malondialdehyde concentration, iron content and reactive oxygen species levels were quantified in the present study. In addition, western blot analysis was conducted to explore the potential mechanisms underlying ACSL4 and ZFTA in the modulation of ferroptosis in HUVECs. The results of the present study demonstrated that the expression levels of ACSL4 and ZFTA were significantly increased in human atherosclerotic plaques. In addition, ACSL4 knockout led to a reduced susceptibility to ferroptosis, while ZFTA contributed to ferroptosis in HUVECs. Results of the present study also demonstrated that ZFTA overexpression upregulated ACSL4 expression in HUVECs, whereas ZFTA knockdown led to decreased ACSL4 expression. Co-transfection experiments demonstrated that the ZTFA overexpression-mediated increase in ferroptosis was reversed following ACSL4 knockdown. Collectively, results of the present study highlighted that ACSL4 mediated the effects of ZFTA on the ferroptosis of HUVECs. Thus, the present study demonstrated the potential role of ACSL4 and ZFTA in the regulation of ferroptosis,
and highlighted that ferroptosis-related pathways may act as potential targets in the treatment of AS.

Introduction

Atherosclerosis (AS) is a prevalent cardiovascular disease characterized by the accumulation of lipid deposits in the arterial walls (1). Endothelial cells (ECs) form a layer of flat cells distributed along the inner walls of blood vessels. The development of AS is closely associated with EC impairment, with programmed cell death emerging as the central mechanism responsible for EC injury, encompassing necrosis, apoptosis and ferroptosis (2,3).

Ferroptosis, a form of programmed cell death, is distinctive due to its iron-dependent lipid peroxidation (4,5). Fe^{2+} oxidizes lipids, leading to the accumulation of reactive oxygen species (ROS), ultimately culminating in oxidative cell death (6,7). Modulating the ferroptosis pathway exhibits potential as a therapeutic strategy for mitigating the progression of various diseases (8). Results of previous studies suggested that ferroptosis plays a significant role in the pathogenesis of AS, through processes involving iron overload, oxidative stress and lipid peroxidation (9-12). Metabolism disorders of iron and lipids are implicated in endothelial cell ferroptosis and vascular toxicity (13). However, the molecular mechanisms underlying ferroptosis in ECs in AS remain to be fully elucidated.

Acyl-CoA synthetase long chain family member 4 (ACSL4), a member of the ACSL family, is predominantly expressed in the endoplasmic reticulum and mitochondrial membranes, catalyzing the metabolism of long-chain free fatty acids into acyl-CoA (14). Results of a previous study revealed that ACSL4 plays a crucial role in promoting ferroptosis through the synthesis of membrane phospholipids. This leads to an increased susceptibility of cells to ferroptosis inducers, such as RSL3 [(1S,3R)-RSL3] (15). However, the regulation of ACSL4 in the pathogenesis of AS remains to be fully elucidated. Zinc finger translocation-associated protein (ZFTA) is a Cys2-His2 (C2H2) zinc finger protein containing 678 amino acids. Results of previous studies demonstrated that ZFTA interacts with various transcriptional coactivators in translocations and is involved in transcriptional regulation (16,17). However, the

Correspondence to: Professor Yan-Wei Hu, Department of Clinical Laboratory, Guangzhou Women and Children Medical Center, Guangzhou Medical University, 9 Jinsui Road, Guangzhou, Guangdong 510600, P.R. China
Email: ywhu0618@163.com

potential role of ZFTA in the formation of atherosclerotic plaques remains unclear. The present study hypothesized that ACSL4 and ZFTA may modulate ferroptosis in endothelial cells , thereby influencing the pathogenesis of AS.

Materials and methods

Human sample. The patient samples and the control samples for this study were collected from the Department of Vascular Surgery, Nanfang Hospital, Southern Medical University, Guangzhou, China, between May 2013 and May 2015. A total of 20 human atherosclerotic plaque samples were obtained from patients undergoing carotid endarterectomy. Control samples were arteries without macroscopic evidence of atherosclerosis, obtained from individuals who died from either a traffic accident or cerebral edema. The plaque tissues were pathologically confirmed as primary atherosclerosis and immediately frozen in liquid nitrogen at -196˚C. Exclusion criteria included diabetes, cancer, congestive heart failure, valvular heart disease, hematological system diseases, auto-immune disease and/or infections. The basic information of the patients included name, age and sex. Ethics approval was obtained from the Ethics Committee of The Women and Children's Medical Center (approval no. 286B01). The present study adhered to the principles outlined in the Declaration of Helsinki. All patients or relatives of deceased individuals provided written informed consent prior to the study.

Cell culture. HUVECs and 293T cells were acquired from the ATCC and cultivated in conditioned high-glucose DMEM (Gibco; Thermo Fisher Scientific, Inc.) with added 10% fetal bovine serum and 100 U/ml penicillin/streptomycin (Invitrogen; Thermo Fisher Scientific, Inc.). HUVECs-LV-ZFTA cells and HUVECs-LV-Mock cells by were isolated by inoculating lentiviruses LV-ZFTA and LV-Mock and selecting with puromycin. All cell lines were sustained in a controlled environment at 37˚C with 5% CO_2.

Lentivirus production and cell line infection. To construct a vector overexpression ZFTA (LV-ZFTA), the ZFTA gene (Gene ID: 65998) was amplified by PCR (Primer forward: 5'-TTGAATTCATGGAGCCCGGCGGGGA-3', reverse: 5'-TTGGATCCCTACGCCCGACACACAGCG-3') and inserted into the *Eco*RI and *Bam*HI restriction enzyme sites of the lentiviral vector CSII-EF-MCS-IRES2-Venus (Riken; cat. no. RDB04384). The CSII-EF-MCS-IRES2-Venus was used as LV-Mock control. For lentivirus production, the generation system used 2nd generation lentiviral system. 293T cells were cultured with DMEM medium and $4x10^6$ cells were seeded per 10-cm dish. On the next day, the cells were transfected with lentivirus plasmids (13 μg), an encoding vesicular stomatitis virus (VSV-G) envelope protein plasmid pMD.2G (6 μg) and a packaging plasmid psPAX2 (12 μg) using the Lipofectamine® 3000 reagent (Invitrogen; Thermo Fisher Scientific, Inc.). Transfection was performed at 37˚C for 6 h. The culturing medium was changed at 6 h post-transfection, and the supernatants were harvested 48 h later. Cell line were established by infecting human HUVECs cells with lentiviruses supernatants at an MOI of 10 with 8 μg/ml polybrene for 24 h, Venus-positive cells were sorted by flow cytometry.

All cell lines were maintained in a humidified atmosphere containing 37˚C and 5% CO_2. Efficient ZFTA overexpression was verified by quantitative RT-PCR (Fig. S1).

CRISPR/Cas9 knockout cells. The CRISPR/Cas9 system was used to generate clones of cells with ACSL4 gene disruptions. ACSL4 single guide (sg)RNAs (5'-aatcgcagagtgaataactt-3' and 5'-tcatgggctaaatgaatctg-3') were designed using CHOPCHOP online tool (http://chopchop.cbu.uib.no/). These sgRNAs were cloned into the lentiCRIPSR v2 vector, which contains the Cas9 gene (cat. no. 52961; Addgene, Inc.). The targeted exon was exon 3 of the ACSL4 gene, which affects the acyl-CoA synthetase domain. 293T cells were used to package the lentivirus. FuGENE HD Reagent (Promega Corporation) was used to introduce 400 ng of lentiCRISPR v2 containing sgRNA, 400 ng of pSPAX2 (cat. no. 12260; Addgene, Inc.) and 200 ng of pMD2G (cat. no. 12259; Addgene, Inc.) into 293T cells (12-well plate). Culture supernatants were filtered through a 0.45 m filter after two days and then used for gene transduction. A lentivirus carrying sgRNA was transduced into HUVEC cells and selected with puromycin (2 μg/ml). Single clones were selected and expanded with mutations characterized as small insertions or deletions (indels), resulting in frameshift mutations that likely disrupt the ACSL4 protein function. Detecting ACSL4 expression by immunoblotting were performed. Cells expressing non-targeting sgRNAs (5'-tgcgaatacgcccacgcgat-3' and 5'-atcgcgtgggcgtattcgca-3') served as a negative control.

Cell viability assays. CCK8 (Cell Counting Kit-8) was purchased from MC Express to measure cell viability. In brief, cells were seeded into 96-well plates and cultured overnight. A glutathione peroxidase 4 inhibitor, RSL-3 (Selleck Chemicals), was then applied to the cells for 24 h. Following treatment for the indicated time points, 10 μl CCK-8 reagent were introduced to each well of the plate, followed by an incubation period at 37˚C for 1 h. Subsequently, the optical density (OD) value was determined using a BioTek Instrument (BioTek China) at 450 nm.

Reverse transcription-quantitative (RT-q) PCR. Total RNA from patient atherosclerotic plaques and HUVECs ($1x10^6$/well in 6-well plates) was extracted using TRIzol® reagent (Invitrogen; Thermo Fisher Scientific, Inc.) according to the manufacturer's protocol. Additionally, 1 μg RNA was reverse transcribed into cDNA using the HI Script Q RT SuperMix (Vazyme Biotech Co., Ltd.) according to the manufacturer's instructions. RT-qPCR was performed using the cDNA templates and SYBR (Takara Bio, Inc.) in a Bio-Rad CFX96 system (Bio-Rad Laboratories, Inc.). The PCR cycling conditions were: denaturation at 95˚C for 30 sec, annealing at 60˚C for 30 sec, and extension at 72˚C for 30 sec, for a total of 40 cycles. Gene expression levels were calculated using the 2-ΔΔCq method, normalized to β-actin, as described by Livak and Schmittgen (18). The experiments were replicated three times. The primers were used in RT qPCR as follows: ACSL4 forward, 5'-CATCCCTGGAGCAGATACTCT-3'; ACSL4 reverse, 5'-TCACTTAGGATTTCCCTGGTCC-3'. ZFTA forward, 5'-CTCAAGGTGAGCACCATCAAG-3'; ZFTA reverse, 5'-GCTCCTCAGGCGTGAAGTC-3'. β-actin

forward, 5'-CCAACCGCGAGAAGATGA-3'; β-actin reverse, 5'-CCAGAGGCGTACAGGGATAG-3'.

Iron content assay. Plaques from human atherosclerosis and pellets from cultured HUVECs were homogenized in saline and PBS, and centrifuged following homogenization. The centrifugation conditions were 10,000 x g, 4°C and a duration of 15 min. Based on the manufacturer's instructions, an Iron Assay Kit (cat. no. TC1015; Leagene; Beijing Regen Biotechnology Co., Ltd.) was used to determine the iron content. The OD value was determined using a BioTek instrument (BioTek China) at 562 nm.

Measurement of lipid peroxidation. Lipid peroxidation was assessed by quantifying MDA concentrations using the thiobarbituric acid (TBA) method, as per commercial recommendations (Nanjing Jiancheng Bioengineering Institute). This method relies on the spectrophotometric measurement of the color generated in the reaction between TBA and malondialdehyde (MDA). MDA concentrations were determined based on the absorbance of TBA reactive substances at 532 nm, measured using a microplate reader (BioTek China).

Immunofluorescence staining. The atherosclerotic plaques derived from the patients were fixed in 4% paraformaldehyde (PFA), dehydrated through ascending ethanol series (70, 80, 95, and 100%), followed by xylene, and then embedded in paraffin wax and sectioned into five μm sections. For tissue cell death detection, In situ Cell Death Detection Kit was used to stain tissue sections; fluorescein was added according to the manufacturer's instructions (cat. no. 11684795910; Roche Diagnostics) at 37°C for 60 min, and DAPI (Thermo Fisher Scientific, Inc.) was used to stain the nucleus at room temperature for 5 min. In order to determine the expression levels of CD31 and ACSL4 in atherosclerotic plaques, antibodies were used as follows: Mouse antihuman CD31 antibody (clone JC/70A; cat. no. ab9498; Abcam) and rabbit antihuman ACSL4 antibody (clone EPR8640; cat. no. ab155282; Abcam). As secondary antibodies, Alexa Fluor 594-conjugated goat anti-rabbit IgG H&L (A-11012, Thermo Fisher Scientific) and Alexa Fluor 488-conjugated goat anti-mouse IgG H&L (A-11001, Thermo Fisher Scientific, Inc.) were used. Images were captured using a fluorescence microscope (DM6000B; Leica Microsystems GmbH).

Western blotting. In order to prepare the whole cell extract, 1 mM PMSF, 1% protease inhibitor cocktail (MilliporeSigma) and dithiothreitol were used. Protein concentration was determined using the Bradford assay, 30 μg of protein was loaded per lane. Proteins were separated by 10% SDS-PAGE and transferred onto nitrocellulose membranes, followed by blocking in 0.1% PBST (PBS with 0.1% Tween 20) with 5% bovine serum albumin (New England BioLabs, Inc.) at room temperature for 1 h. The membranes were then incubated with primary antibodies at 4°C overnight. Primary antibodies included anti-tubulin antibody (1:5,000; cat. no. RM2007; BBI Life Sciences) and anti-ACSL4 antibody (1:10,000; cat. no. EPR8640; Abcam). Membranes were incubated with IRDye 800 CW-conjugated anti-rabbit-IgG and IRDye 680 LT-conjugated anti-mouse-IgG secondary antibodies (LI-COR Biosciences) at room temperature for 1 h. Immunoreactive bands were visualized using an Odyssey infrared imaging system (LI-COR Biosciences). Densitometry was performed using Image Studio software, version 5.2 (LI-COR Biosciences).

RNA interference. The small interfering RNAs (siRNAs) were sourced from Guangzhou RiboBio Co., Ltd. The sequences of siRNAs targeting human ZFTA mRNA and ACSL4 mRNA were 5'-GCACAGUUAUGCUGUACAACU-3' and 5'-GAG CGAUUUGAAAUUCCAA-3', respectively. A control siRNA with scrambled sequence was used as a negative control (cat. no. siN0000001-1-5). Cells were transfected with siRNAs or a negative control using Lipofectamine® 3000 reagent (cat. no. L3000015; Invitrogen; Thermo Fisher Scientific, Inc.), following the manufacturer's instructions. Transfection was performed at 37°C for 48 h. Following transfection, a 48-h interval was allowed before subsequent experimentation. Subsequently, RT-qPCR was conducted to assess knockdown efficiencies as above.

Detection of reactive oxygen species (ROS). Lipid ROS levels in HUVECs were assessed using C11-BODIPY581/591 (cat. no. D3861; Gibco; Thermo Fisher Scientific, Inc.). Following treatment and culture, cells were washed with PBS and labeled with C11-BODIPY581/591 (5 mM) for 15 min at 37°C in the dark. The lipid ROS levels were then observed under a fluorescence microscope.

Transmission electron microscopy (TEM) analysis. The atherosclerotic plaques derived from the patients were cut into 1 mm³ blocks and fixed in 4% paraformaldehyde. After washing with 0.1 M phosphate buffer (PB, pH 7.4), samples were post-fixed in 1% osmium tetroxide for 2 h at room temperature. Dehydration was carried out through graded ethanol (30, 50, 70, 80, 95, and 100%) and acetone. Samples were then infiltrated with acetone and EMBed 812 resin mixtures, embedded in pure resin and polymerized at 65°C for 48 h. Ultrathin sections (60-80 nm) were cut using an ultra-microtome (Leica UC7) and placed on 150 mesh copper grids. Sections were stained with 2% uranyl acetate and 2.6% lead citrate, then observed under a HITACHI HT7800 TEM.

Fluorescence in situ hybridization. HUVECs cells were cultured on glass coverslips until reaching 70-80% confluence, then fixed in 4% paraformaldehyde at room temperature. The cells were permeabilized with 0.5% Triton X-100 for 10 min. A FAM-labeled probe specific for ZFTA was denatured at 75°C for 5 min and hybridized to the cells at 37°C for 16 h. After hybridization, cells were washed with 2x SSC at 42°C for 10 min, 1x SSC at 42°C for 10 min, and 0.5x SSC at room temperature for 5 min. Nuclei were counterstained with DAPI at room temperature for 5 min, then examined under a fluorescence microscope (cat. no. DM6000B; Leica Microsystems GmbH).

TUNEL staining. Tissues were fixed in 4% paraformaldehyde in PBS for 15 min and washed with PBS. Samples were permeabilized with 20 μg/ml Proteinase K for 10 min. TUNEL reaction mix (cat. no. 11684795910; Roche Diagnostics) was
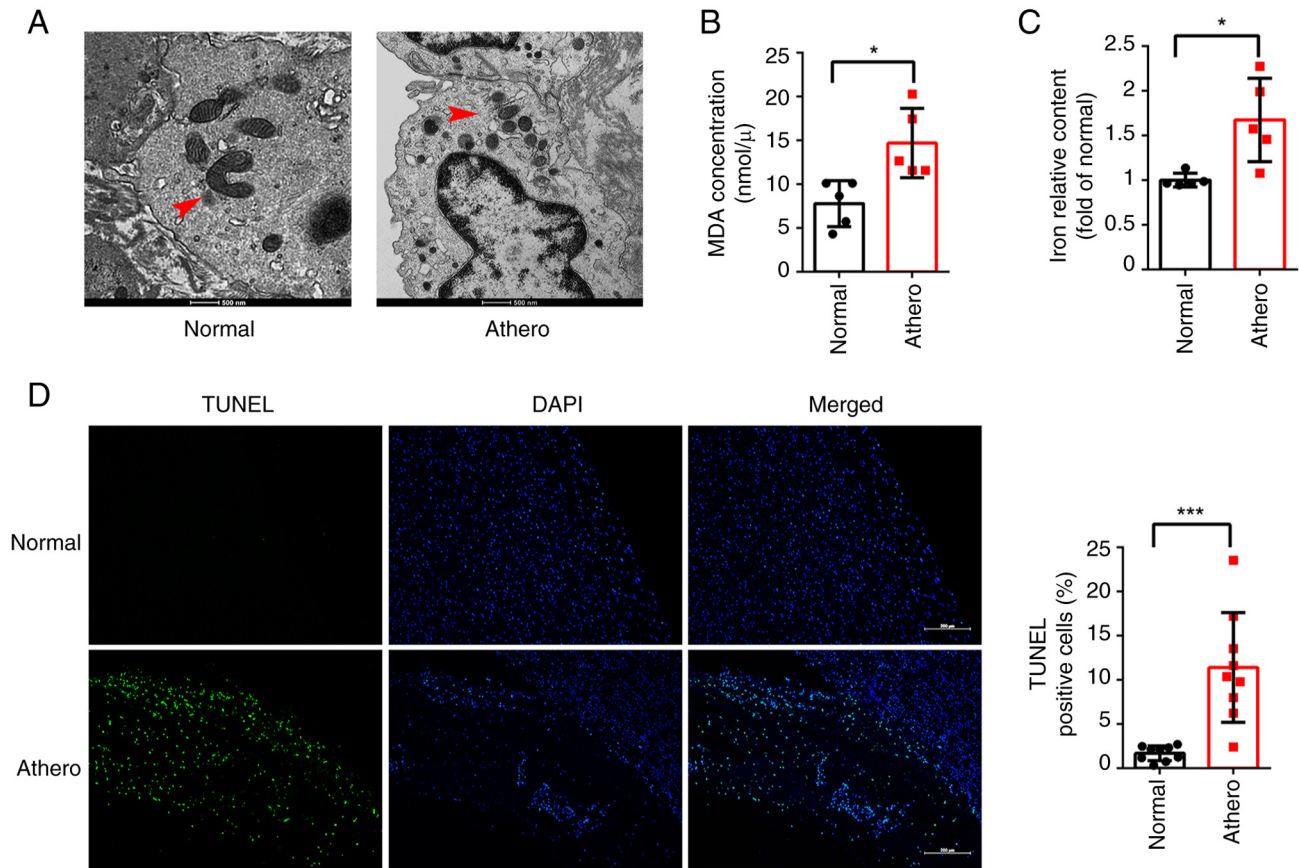
Figure 1. Detection of ferroptosis in atherosclerotic plaques. (A) The morphology of mitochondria in human atherosclerotic plaques was examined using TEM. (B) The content of MDA, the end product of lipid peroxidation, was compared between human atherosclerotic plaques (n=5) and healthy artery tissues (n=5) using commercial kits. (C) The iron levels in the atherosclerotic plaques (n=5) and healthy arterial tissue (n=5) were measured by commercial kits. (D) Cell death was compared between atherosclerotic plaques (n=8) and healthy tissue (n=8) using TUNEL staining. Fluorescence microscopy image at 20x magnification. *P<0.05, ***P<0.001. TEM, transmission electron microscopy; MDA, malondialdehyde; athero, atherosclerotic plaques.

added according to the kit instructions and incubated at 37°C in the dark for 60 min. After PBS washes, samples were counterstained with 1 µg/ml DAPI for 5 min. The sections were then washed, mounted, and examined under a fluorescence microscope (DM6000B; Leica Microsystems GmbH) to identify death cells.

Spearman correlation analysis based on TCGA database data. First, input files containing gene expression data from different cancer types were prepared, selecting the gene pair ZFTA and ACSL4. The working directory was set, and the input files were read to extract the gene expression data. The Spearman method was then used to calculate the correlation coefficient and P-value between the gene expression data. Finally, the ggplot2 package was used to draw a scatter plot, adding regression lines and correlation coefficients for visualization.

Statistical analysis. All experiments were independently replicated a minimum of three times. Data analysis was carried out using GraphPad Prism 7.0 (Dotmatics) and the results were expressed as mean ± SEM. Statistical significance was determined through a one-way ANOVA with Dunnett's test or a two-way ANOVA analysis. Significance levels were denoted as follows: *P<0.05, **P<0.01, ***P<0.001, ****P<0.0001. P<0.05 was considered to indicate a statistically significant difference.

Results

The present study investigated the role of ACSL4 and ZFTA in regulating endothelial cell ferroptosis in AS. It was hypothesized that ACSL4 and ZFTA may modulate ferroptosis in endothelial cells and contribute to AS pathogenesis. Results of the present study demonstrated that ACSL4 is associated with ferroptosis in human AS plaques, as ACSL4 knockdown significantly inhibited the ferroptosis of HUVECs. In addition, ZFTA expression was increased in atherosclerotic plaques, and the ferroptosis of HUVECs was increased following increased ACSL4 expression. Collectively, the findings of the present study revealed that ZFTA may initiate endothelial cell ferroptosis through the regulation of ACSL4, thus, leading to the occurrence and further development of AS.

Ferroptosis in human atherosclerotic plaques. Mitochondrial damage is indicative of ferroptosis (19). Results of transmission electron microscopy (TEM) demonstrated consistent morphological changes in the mitochondria during ferroptosis in human atherosclerotic plaques, including mitochondria shrinkage, cristae lysis and the increased density of the mitochondrial outer membrane (Fig. 1A). To further demonstrate the presence of ferroptosis in human atherosclerotic plaques, lipid peroxidation and iron content was compared between
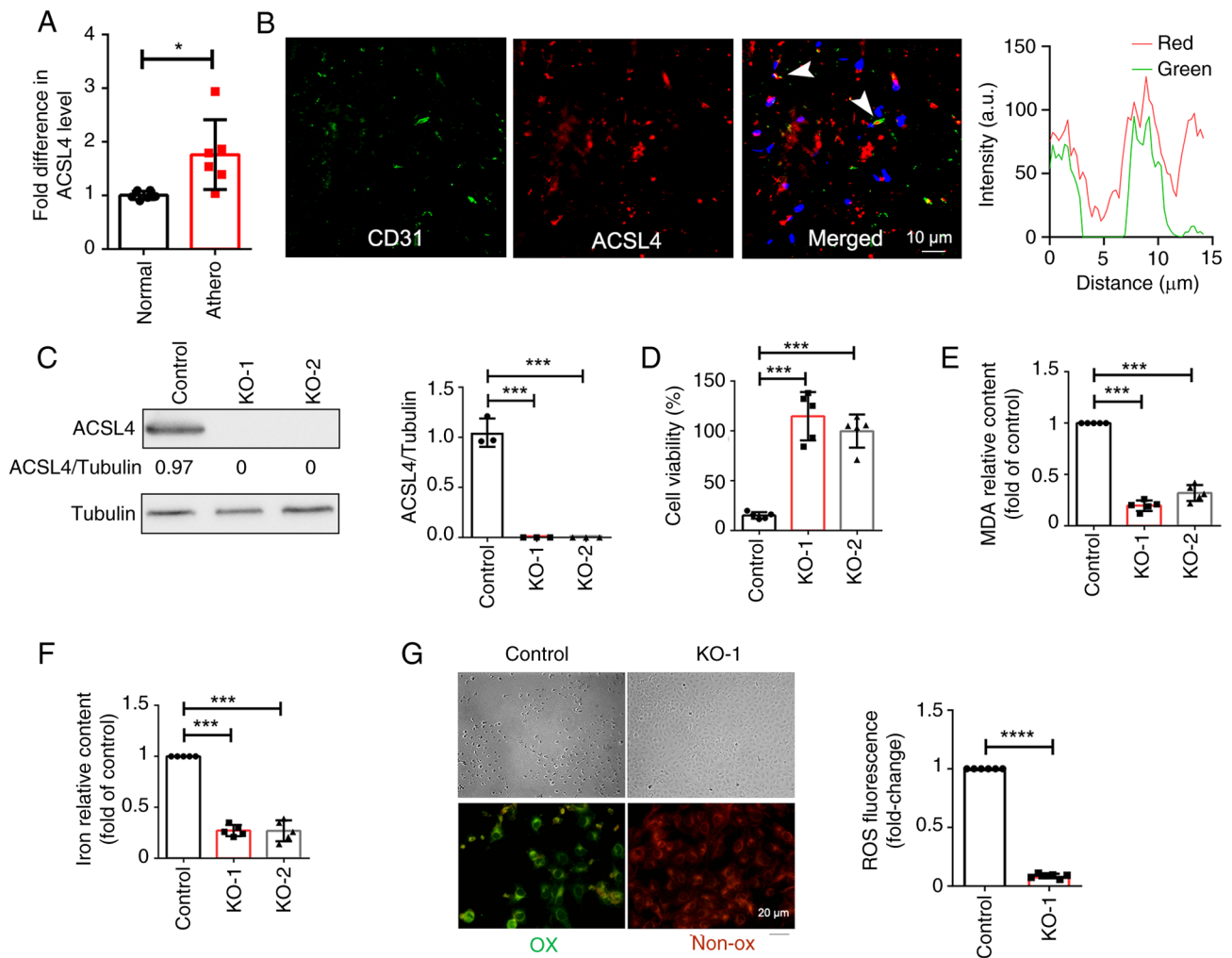
Figure 2. ACSL4 promotes the ferroptosis of endothelial cells. (A) The mRNA levels of ACSL4 were measured using RT-qPCR in human atherosclerotic plaques (n=6) and healthy arterial tissues (n=6). (B) Immunofluorescence staining revealed the co-localization of ACSL4 and the endothelial cell marker CD31 in human atherosclerotic plaques. (C) ACSL4 expression was determined in knockout and control cells using western blot analysis (D) Cell viability was determined in knockout and control cells using a CCK-8 assay. (E) MDA levels and (F) Iron content were significantly reduced in knockout cells, compared with controls. (G) Control and knockout cells were treated with 2 μM RSL3 for 75 min, and active oxygen was labeled with BODIPY 581/591 C11 before imaging (green, oxidized; red, non-oxidized). $^*P<0.05$, $^{***}P<0.001$, $^{****}P<0.0001$. ACSL4, acyl-CoA synthetase long chain family member 4; RT-qPCR, reverse transcription-quantitative PCR; KO, knockout; CCK-8, Cell Counting Kit-8; RSL3, (1S,3R)-RSL3; athero, atherosclerotic plaques.

five human atherosclerotic plaques and five human healthy tissues. The results revealed a substantial increase in both MDA and iron contents within human atherosclerotic plaques compared with healthy tissues (Fig. 1B and C). Subsequently, cell death was examined in eight human atherosclerotic plaque and eight human healthy control tissues using TUNEL staining, and the results demonstrated a significant increase in cell death in atherosclerotic plaques (Fig. 1D). These findings highlight the role of ferroptosis in the development and progression of AS.

Elevation of ACSL4 in human atherosclerotic plaques and inhibition of ferroptosis of HUVECs by knockout of ACSL4. Results of the present study revealed that ACSL4 plays a role in ferroptosis. ACSL4 mRNA expression was compared between six atherosclerotic plaques and six healthy controls obtained from human samples. Results revealed that ACSL4 mRNA expression levels were significantly increased in human atherosclerotic plaques compared with healthy tissues

(Fig. 2A). Immunofluorescence was subsequently carried out to determine the localization of ACSL4 in atherosclerotic plaques, and the results demonstrated that ACSL4 was predominantly expressed within the HUVECs (Fig. 2B).

To verify the role of ACSL4 in the ferroptosis of HUVECs, CRISPR/Cas9 was used for ACSL4 knockout in HUVECs and two monoclonal cell lines with ACSL4 knockout were screened. ACSL4 knockout in HUVECs was confirmed via western blot analysis (Fig. 2C). Ferroptosis was induced in HUVECs using RSL3, and cell survival, MDA content, iron content and OS) levels were compared between ACSL4 knockout cells and controls. The results of the present study demonstrated that ACSL4 knockout significantly improved cell survival (Fig. 2D), reduced the levels of MDA, an end product of lipid peroxidation (Fig. 2E), reduced iron content (Fig. 2F) and decreased the levels of ROS (Fig. 2G), compared with control cells. Collectively, these findings indicated that ACSL4 knockout effectively inhibited the ferroptosis of HUVECs.
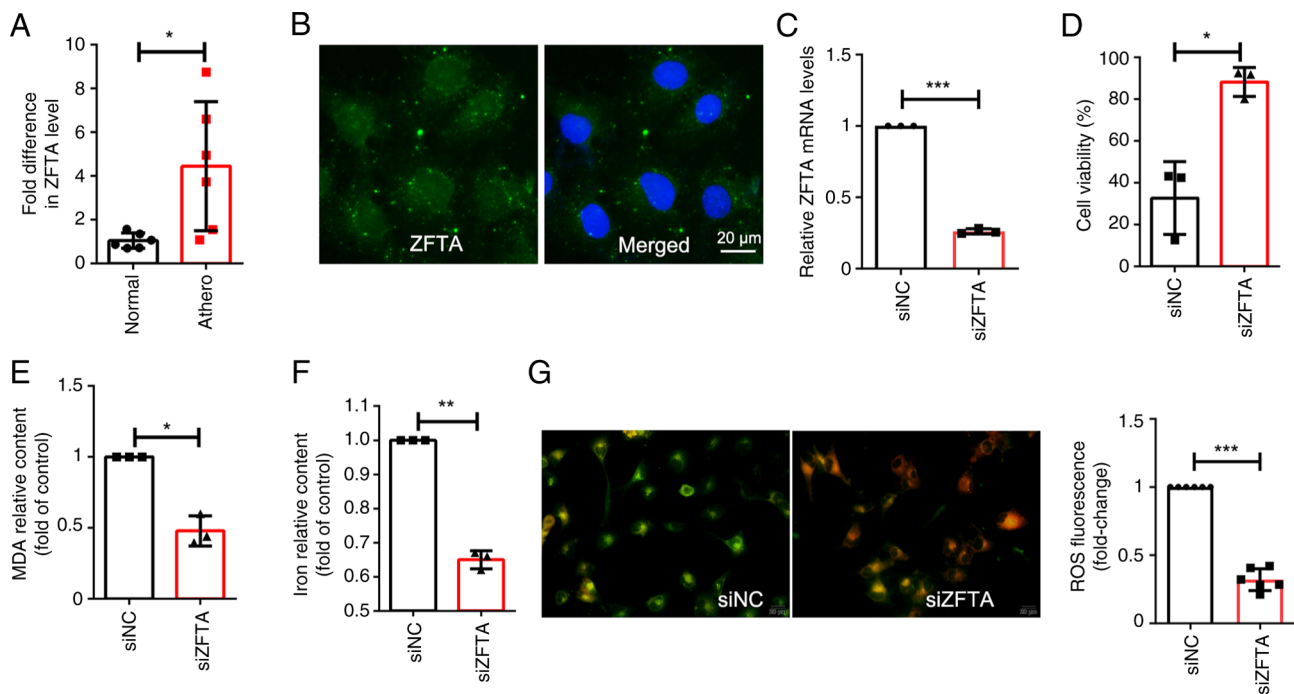
Figure 3. ZFTA promotes the ferroptosis of endothelial cells. (A) ZFTA mRNA expression levels were measured using RT-qPCR in human atherosclerotic plaques (n=6) and healthy arterial tissues (n=6). (B) Fluorescence *in situ* hybridization was used to determine the localization of ZFTA in HUVECs. (C) Cells were transfected with siRNA with scrambled sequence (siNC), or siRNAs against ZFTA (siZFTA), mRNA expression levels of ZFTA were measured using RT-qPCR. (D) Cell viability was determined using a CCK-8 assay following ZFTA knockdown and RSL3 treatment in endothelial cells. (E) The levels of MDA were significantly reduced in cells following transfection with siZFTA, compared with cells transfected with siNC. (F) Iron content was significantly reduced in cells following transfection with siZFTA, compared with cells transfected with siNC. (G) siNC and siZFTA cells were treated with 2 μM RSL3 for 75 min, and active oxygen was labeled with BODIPY 581/591 C11 before imaging. (Green, oxidized; red, non-oxidized). *P<0.05, **P<0.01 and ***P<0.001. ZFTA, zinc finger translocation-associated protein; RT-qPCR, reverse transcription-quantitative PCR; HUVECs, human umbilical vein endothelial cells; CCK-8, Cell Counting Kit-8; RSL3,; siRNA, small interfering RNA; NC, negative control.

Increased ZFTA in human atherosclerotic plaques and ZFTA silencing suppresses ferroptosis of HUVECs. ZFTA (C11orf95) is a functionally unknown gene that binds to various transcriptional coactivators in translocations. RT-qPCR was performed using six atherosclerotic plaques and six healthy control tissues. Results of the present study indicated a significant upregulation in ZFTA RNA expression levels in atherosclerotic plaques, compared with healthy arterial tissues (Fig. 3A). ZFTA localization was determined using fluorescence *in situ* hybridization (FISH) analysis and the results demonstrated that ZFTA was expressed in both the cytoplasm and the nucleus of HUVECs (Fig. 3B). Cells were transfected with ZFTA siRNA (siZFTA) and viability, MDA content, iron content and ROS levels were compared between siZFTA and negative control (siNC) cells, following the RSL3-mediated induction of ferroptosis. Compared with siNC cells, transfection with siZFTA significantly increased cell viability, reduced MDA content, decreased iron content and reduced ROS levels, indicating that ZFTA knockdown may suppress ferroptosis in HUVECs (Fig. 3C-G).

ACSL4 knockdown reverses the promoting effect of ZFTA overexpression on endothelial cell ferroptosis. TCGA database revealed a significant positive correlation between the expression of ZFTA-ACSL4 in various tumor types, including prostate adenocarcinoma and pancreatic adenocarcinoma (Fig. S2). To further verify the role of ZFTA in the regulation of ACSL4 expression, cells were transfected with siZFTA.

Results revealed that ACSL4 mRNA and protein expression levels were decreased following ZFTA knockdown (Fig. 4A and B). The present study also demonstrated that ZFTA overexpression significantly increased the mRNA and protein expression levels of ACSL4 (Fig. 4C and D), indicating that ZFTA may promote the expression of ACSL4.

To explore the potential association between ACSL4 and ZFTA in the ferroptosis of ECs, rescue experiments were conducted following the co-transfection of LV-ZFTA and si-ACSL4 in HUVECs. Results of the present study revealed that ACSL4 knockdown reversed ZFTA overexpression-mediated ferroptosis (Fig. 4E-G). Therefore, ACSL4 may mediate the regulation of ZFTA in the ferroptosis of HUVECs.

Discussion

Ferroptosis, a form of programmed cell death, is distinctive due to its iron-dependent lipid peroxidation. Manifestation of ferroptosis includes mitochondrial structural abnormalities and increased levels of iron and lipid peroxides (19). AS is associated with the accumulation of lipids within the walls of medium and large-sized arteries. Results of previous studies suggest a potential association between ferroptosis and various cellular pathological processes that influence the initiation and advancement of AS. These processes encompass disruptions in lipid and iron metabolism, oxidative stress and inflammatory responses (9,20-22). Zhou et al (23) revealed the differential expression of ferroptosis-associated genes within human
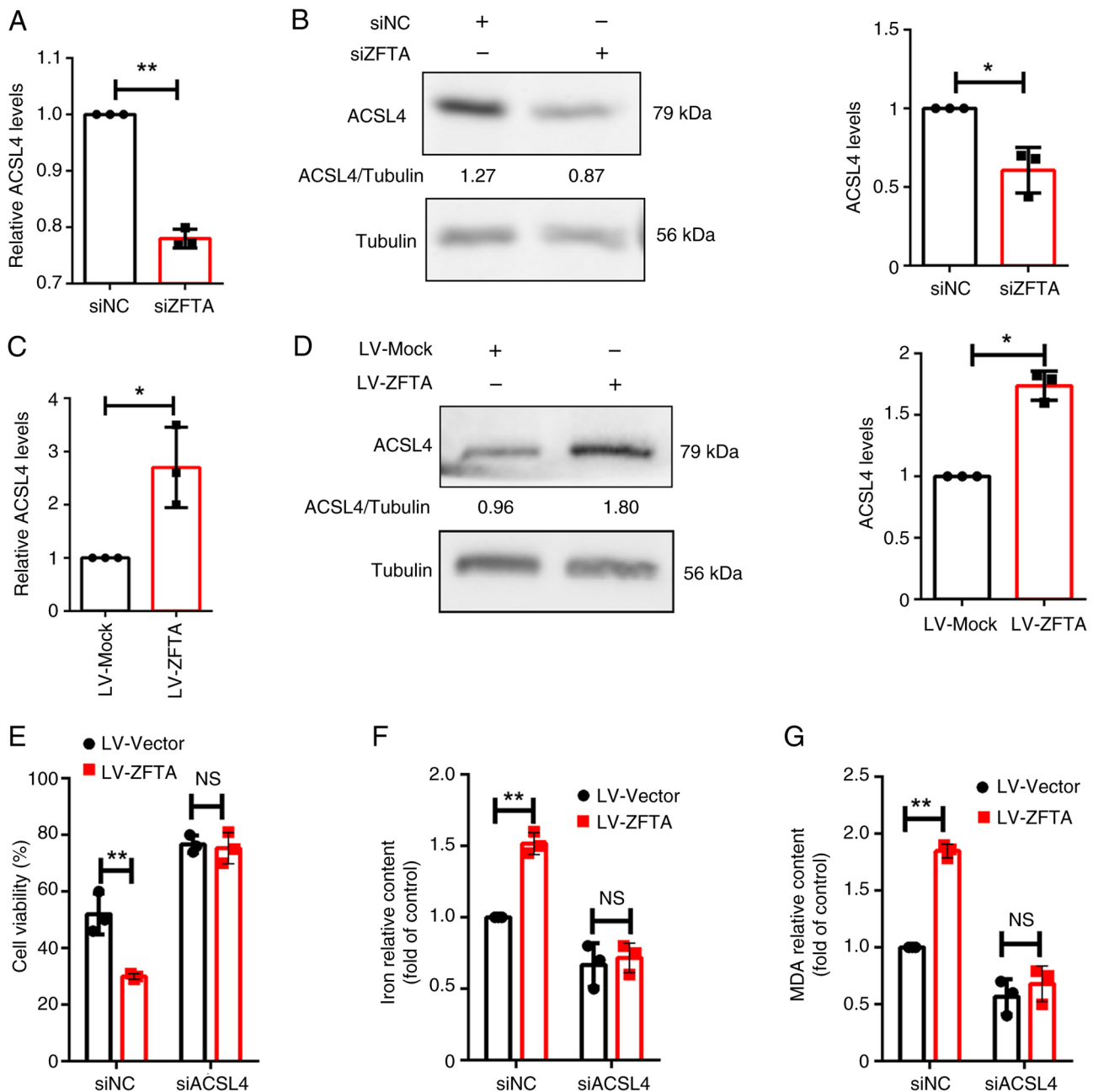
Figure 4. Regulation of ZFTA and ACSL4 in ferroptosis. (A) Following ZFTA knockdown, ACSL4 mRNA levels were measured using RT-qPCR. (B) Following ZFTA knockdown, western blot analysis was performed to assess the protein expression levels of ACSL4, with Tubulin as the internal reference protein. (C) Following ZFTA overexpression, ACSL4 mRNA levels were measured using RT-qPCR. (D) Following ZFTA overexpression, western blot analysis was performed to assess the protein expression levels of ACSL4, with Tubulin as the internal reference protein. Cells with ACSL4 knockdown and ZFTA overexpression were treated with 2 μM RSL3 for 24 h. (E) Cell viability, (F) iron content and (G) MDA levels were measured. $^{*}P<0.05$, $^{**}P<0.01$. ZFTA, zinc finger translocation-associated protein; ACSL4, acyl-CoA synthetase long chain family member 4; RT-qPCR, reverse transcription-quantitative PCR; RSL3; MDA, malondialdehyde; siRNA, small interfering RNA; NC, negative control.

coronary arteries, which was positively correlated with the severity of AS (23). The present study provided evidence for the role of ferroptosis in human AS. Morphological changes in mitochondria were observed within human atherosclerotic plaques and these results were indicative of ferroptosis, including mitochondrial shrinkage, cristae lysis and increased mitochondrial outer membrane density. In addition, the results of the present study demonstrated elevated levels of MDA and iron content in human atherosclerotic plaques. These results suggested that ferroptosis may play a crucial role in the development and progression of AS. However, the underlying

molecular mechanisms of ferroptosis in AS remain to be elucidated.

ECs form the inner lining of blood vessels, and ferroptosis of these cells may promote endothelial dysfunction, leading to lipid accumulation within arterial vessel walls, ultimately contributing to AS (13,24,25). The administration of iron chelators in mice inhibits EC ferroptosis, mitigates EC dysfunction and consequently slows the progression of AS (26). Thus, targeting the regulation of endothelial ferroptosis may exhibit potential in the treatment of AS. ACSL4 is a biomarker of pathological ferroptosis (27,28). Previous studies on the involvement

of ACSL4 in AS primarily focused on ACSL4 expression profiling and functional analysis (23,29,30). However, the regulatory functions of ACSL4 remain to be fully elucidated. The present study highlighted the key role of ACSL4 in both human atherosclerotic plaques and the ferroptosis of ECs. The results revealed a significant increase in the ACSL4 mRNA expression levels in human atherosclerotic plaques and ACSL4 localization was further confirmed using immunofluorescence. Moreover, using CRISPR/Cas9-technology in HUVECs, results of the present study demonstrated that ACSL4 knockout increased cell survival rates, reduced the levels of MDA, decreased iron content and reduced ROS levels following the induction of ferroptosis. Collectively, the results of the present study demonstrated that ACSL4 expression may be associated with the initiation and development of ferroptotic cell death. Monitoring ACSL4 protein levels may be a suitable diagnostic approach for AS.

ZFTA is a zinc finger protein, and the regulatory molecular mechanism remains elusive. Previous studies demonstrated that ZFTA expression leads to continual nuclear translocation, potentially playing a role in unique DNA binding and transcriptional regulation (16,17). In addition, ZFTA collaborates with diverse transcriptional coactivators in various translocation events (31). The results of the present study revealed that ZFTA was significantly upregulated in atherosclerotic plaques, compared with healthy arterial tissues. FISH analysis revealed that ZFTA was expressed in both the cytoplasm and nucleus of ECs. In addition, ZFTA knockdown led to increased cell viability, decreased MDA content, reduced iron content and reduced ROS levels in ECs following the induction of ferroptosis. These results highlight the role of ZFTA in promoting ferroptosis in ECs.

The present study revealed the association between ZFTA and ACSL4 and highlighted their interaction in the regulation of ferroptosis. ZFTA knockdown resulted in a decrease in ACSL4 mRNA and protein expression levels, suggesting that ZFTA positively modulated the expression of ACSL4. Conversely, overexpression of ZFTA led to an increase in ACSL4 mRNA and protein expression levels. To investigate whether ACSL4 plays a role in the ZFTA-mediated regulation of ferroptosis of ECs, rescue experiments were conducted. Co-transfection of ZFTA overexpression vectors and siACSL4 in ECs demonstrated that ACSL4 knockdown reversed the ferroptosis-inducing effects of ZFTA overexpression. These results demonstrated that ACSL4 may act as a mediator in the ZFTA-mediated regulation of ferroptosis in ECs.

The findings of the present study have to be seen in light of some limitations. The first is the absence of further investigation into the underlying mechanism of the interaction between ZFTA and ACSL4 proteins. Future studies employing techniques such as co-immunoprecipitation could provide insights into the nature of this interaction, including the binding domains involved. Secondly, due to the small sample size, the reliability and accuracy of the study will be affected. In future studies, more specimens will be collected for further verification.

In conclusion, results of the present study preliminarily revealed the complex molecular mechanism underlying ferroptosis in human atherosclerotic plaques. The pivotal roles of ACSL4 and ZFTA in the ferroptosis of ECs may uncover potential therapeutic targets for managing AS and associated cardiovascular diseases. Further investigations are required to explore the specific mechanisms and potential targets of ferroptosis, which may aid in the development of innovative clinical treatment strategies.

Acknowledgements

Availability of data and materials

The data generated in the present study may be requested from the corresponding author.

Authors' contributions

YWH designed the study. HXG, JJ, CY, JFX and QH conducted the experiments and acquired and analyzed the data. HXG wrote the manuscript. YWH and HXG revised the manuscript. All authors read and approved the final manuscript. HXG and JJ confirm the authenticity of all the raw data.

Ethics approval and consent to participate

Ethics approval was obtained from the Ethics Committee of The Women and Children's Medical Center (approval no. 286B01). The present study adhered to the principles outlined in the Declaration of Helsinki. All patients or relatives of deceased individuals provided written informed consent prior to the study.

Patient consent for publication

Not applicable.

Competing interests

The authors declare that they have no competing interests.

References

1. Libby P: The changing landscape of atherosclerosis. Nature 592: 524-533, 2021.
2. Gimbrone MA Jr and García-Cardeña G: Endothelial cell dysfunction and the pathobiology of atherosclerosis. Circ Res 118: 620-636, 2016.
3. Lin L, Zhang MX, Zhang L, Zhang D, Li C and Li YL: Autophagy, pyroptosis, and ferroptosis: New regulatory mechanisms for atherosclerosis. Front Cell Dev Biol 9: 809955, 2021.
4. Yu H, Guo P, Xie X, Wang Y and Chen G: Ferroptosis, a new form of cell death, and its relationships with tumourous diseases. J Cell Mol Med 21: 648-657, 2017.

5. Latunde-Dada GO: Ferroptosis: Role of lipid peroxidation, iron and ferritinophagy. Biochim Biophys Acta Gen Subj 1861: 1893-1900, 2017.
6. Stockwell BR, Friedmann Angeli JP, Bayir H, Bush AI, Conrad M, Dixon SJ, Fulda S, Gascón S, Hatzios SK, Kagan VE, et al: Ferroptosis: A regulated cell death nexus linking metabolism, redox biology, and disease. Cell 171: 273-285, 2017.
7. Xu S, Min J and Wang F: Ferroptosis: An emerging player in immune cells. Sci Bulletin (Beijing) 66: 2257-2260, 2021.
8. Li J, Cao F, Yin HL, Huang ZJ, Lin ZT, Mao N, Sun B and Wang G: Ferroptosis: Past, present and future. Cell Death Dis 11: 88, 2020.
9. Wang Y, Zhao Y, Ye T, Yang L, Shen Y and Li H: Ferroptosis signaling and regulators in atherosclerosis. Front Cell Dev Biol 9: 809457, 2021.
10. Yu Y, Yan Y, Niu F, Wang Y, Chen X, Su G, Liu Y, Zhao X, Qian L, Liu P and Xiong Y: Ferroptosis: A cell death connecting oxidative stress, inflammation and cardiovascular diseases. Cell Death Discov 7: 193, 2021.
11. Cornelissen A, Guo L, Sakamoto A, Virmani R and Finn AV: New insights into the role of iron in inflammation and atherosclerosis. EBioMedicine 47: 598-606, 2019.
12. Fang X, Ardehali H, Min J and Wang F: The molecular and metabolic landscape of iron and ferroptosis in cardiovascular disease. Nat Rev Cardiol 20: 7-23, 2023.
13. Lin X, Ouyang S, Zhi C, Li P, Tan X, Ma W, Yu J, Peng T, Chen X, Li L and Xie W: Focus on ferroptosis, pyroptosis, apoptosis and autophagy of vascular endothelial cells to the strategic targets for the treatment of atherosclerosis. Arch Biochem Biophys 715: 109098, 2022.
14. Kuwata H and Hara S: Role of acyl-CoA synthetase ACSL4 in arachidonic acid metabolism. Prostaglandins Other Lipid Mediat 144: 106363, 2019.
15. Lin Z, Liu J, Long F, Kang R, Kroemer G, Tang D and Yang M: The lipid flippase SLC47A1 blocks metabolic vulnerability to ferroptosis. Nat Commun 13: 7965, 2022.
16. Ozawa T, Kaneko S, Szulzewsky F, Qiao Z, Takadera M, Narita Y, Kondo T, Holland EC, Hamamoto R and Ichimura K: C11orf95-RELA fusion drives aberrant gene expression through the unique epigenetic regulation for ependymoma formation. Acta Neuropathol Commun 9: 36, 2021.
17. Zhu JJ, Jillette N, Li XN, Cheng AW and Lau CC: C11orf95-RELA reprograms 3D epigenome in supratentorial ependymoma. Acta Neuropathol 140: 951-960, 2020.
18. Livak KJ and Schmittgen TD: Analysis of relative gene expression data using real-time quantitative PCR and the 2(-Delta Delta C(T)) method. Methods 25: 402-408, 2001.
19. Dixon SJ, Lemberg KM, Lamprecht MR, Skouta R, Zaitsev EM, Gleason CE, Patel DN, Bauer AJ, Cantley AM, Yang WS, et al: Ferroptosis: An iron-dependent form of nonapoptotic cell death. Cell 149: 1060-1072, 2012.
20. Liu W, Östberg N, Yalcinkaya M, Dou H, Endo-Umeda K, Tang Y, Hou X, Xiao T, Fidler TP, Abramowicz S, et al: Erythroid lineage Jak2V617F expression promotes atherosclerosis through erythrophagocytosis and macrophage ferroptosis. J Clin Invest 132: e155724, 2022.
21. Zhang J, Wang X, Guan B, Wang X, An X, Wang T, Chen X, Zhao L, Jia J, Song L, et al: Qing-Xin-Jie-Yu Granule inhibits ferroptosis and stabilizes atherosclerotic plaques by regulating the GPX4/xCT signaling pathway. J Ethnopharmacol 301: 115852, 2023.
22. Su G, Yang W, Wang S, Geng C and Guan X: SIRT1-autophagy axis inhibits excess iron-induced ferroptosis of foam cells and subsequently increases IL-1B and IL-18. Biochem Biophys Res Commun 561: 33-39, 2021.
23. Zhou Y, Zhou H, Hua L, Hou C, Jia Q, Chen J, Zhang S, Wang Y, He S and Jia E: Verification of ferroptosis and pyroptosis and identification of PTGS2 as the hub gene in human coronary artery atherosclerosis. Free Radic Biol Med 171: 55-68, 2021.
24. Zheng D, Liu J, Piao H, Zhu Z, Wei R and Liu K: ROS-triggered endothelial cell death mechanisms: Focus on pyroptosis, parthanatos, and ferroptosis. Front Immunol 13: 1039241, 2022.
25. Yang K, Song H and Yin D: PDSS2 inhibits the ferroptosis of vascular endothelial cells in atherosclerosis by activating Nrf2. J Cardiovasc Pharmacol 77: 767-776, 2021.
26. Bai T, Li M, Liu Y, Qiao Z and Wang ZJ: Inhibition of ferroptosis alleviates atherosclerosis through attenuating lipid peroxidation and endothelial dysfunction in mouse aortic endothelial cell. Free Radic Biol Med 160: 92-102, 2020.
27. Doll S, Proneth B, Tyurina YY, Panzilius E, Kobayashi S, Ingold I, Irmler M, Beckers J, Aichler M, Walch A, et al: ACSL4 dictates ferroptosis sensitivity by shaping cellular lipid composition. Nat Chem Biol 13: 91-98, 2017.
28. Dixon SJ, Winter GE, Musavi LS, Lee ED, Snijder B, Rebsamen M, Superti-Furga G and Stockwell BR: Human haploid cell genetics reveals roles for lipid metabolism genes in nonapoptotic cell death. ACS Chem Biol 10: 1604-1609, 2015.
29. Xiao FJ, Zhang D, Wu Y, Jia QH, Zhang L, Li YX, Yang YF, Wang H, Wu CT and Wang LS: miRNA-17-92 protects endothelial cells from Erastin-induced ferroptosis through targeting the A20-ACSL4 axis. Biochem Biophys Res Commun 515: 448-454, 2019.
30. Zhang M, Yu Z, Zhao L and Luo H: Long non-coding RNA PVT1 regulates atherosclerosis progression via the microRNA-106b-5p/ACSL4 axis. Biochem Biophys Res Commun 667: 170-179, 2023.
31. Parker M, Mohankumar KM, Punchihewa C, Weinlich R, Dalton JD, Li Y, Lee R, Tatevossian RG, Phoenix TN, Thiruvenkatam R, et al: C11orf95-RELA fusions drive oncogenic NF-κB signalling in ependymoma. Nature 506: 451-455, 2014.